

Multi-fidelity Bayesian Optimization with Max-value Entropy Search

Shion Takeno¹, Hitoshi Fukuoka², Yuhki Tsukada³, Toshiyuki Koyama⁴, Motoki Shiga⁵,
Ichiro Takeuchi⁶, and Masayuki Karasuyama⁷

^{1,6,7}Nagoya Institute of Technology

^{2,3,4}Nagoya University

^{3,5,7}Japan Science and Technology Agency

⁵Gifu University

^{6,7}National Institute for Material Science

^{5,6}RIKEN Center for Advanced Intelligence Project

takeno.s.mllab.nit@gmail.com, fukuoka.hitoshi@j.mbox.nagoya-u.ac.jp,
{tsukada.yuhki,koyama.toshiyuki}@material.nagoya-u.ac.jp, shiga_m@gifu-u.ac.jp,
{takeuchi.ichiro,karasuyama}@nitech.ac.jp

Abstract

Bayesian optimization (BO) is an effective tool for black-box optimization in which objective function evaluation is usually quite expensive. In practice, lower fidelity approximations of the objective function are often available. Recently, *multi-fidelity Bayesian optimization* (MFBO) has attracted considerable attention because it can dramatically accelerate the optimization process by using those cheaper observations. We propose a novel information theoretic approach to MFBO. Information-based approaches are popular and empirically successful in BO, but existing studies for information-based MFBO are plagued by difficulty for accurately estimating the information gain. Our approach is based on a variant of information-based BO called *max-value entropy search* (MES), which greatly facilitates evaluation of the information gain in MFBO. In fact, computations of our acquisition function is written analytically except for one dimensional integral and sampling, which can be calculated efficiently and accurately. We demonstrate effectiveness of our approach by using synthetic and benchmark datasets, and further we show a real-world application to materials science data.

1 Introduction

Bayesian optimization (BO) is a popular machine-learning technique for black-box optimizations. The effectiveness of BO has been widely shown in a variety of application areas such as scientific experiments (Wigley et al., 2016), simulation calculations (Ramprasad et al., 2017), and hyperparameter tuning of machine-learning methods (Snoek et al., 2012). In these scenarios, observing an objective function value is usually quite expensive and thus achieving the optimal value with low querying cost is strongly demanded.

Although standard BO only considers directly querying to an objective function $f(\mathbf{x})$, in many practical situations, lower fidelity approximations of the original objective function can be observed. For example, theoretical computations of physical processes often have multiple levels of approximations by which the trade-off between the computational cost and accuracy can be controlled. A goal of *multi-fidelity Bayesian optimization* (MFBO) is to accelerate BO by utilizing those lower fidelity observations to reduce the total cost of the optimization.

Multiple-fidelity sequential kriging optimization (MF-SKO) proposed by (Huang et al., 2006) is a seminal work of MFBO in which the standard expected improvement (EI) is extended to the multi-fidelity setting. A variety of acquisition functions have been studied subsequently. *Gaussian process upper confidence bound* (GP-UCB) is a widely accepted acquisition function in BO (Srinivas et al., 2010), and Kandasamy et al. (2016, 2017) proposed multi-fidelity extensions of GP-UCB. However, all of these approaches have a parameter for balancing exploit-explore trade-off which is usually difficult to tune. Furthermore, in these frameworks, it is difficult to directly evaluate benefit of lower fidelity observations. MF-SKO designs a reward of observing different levels of fidelity heuristically, but no rigorous justification is provided for their acquisition function. In UCB-based approaches (Kandasamy et al., 2016, 2017), the input \mathbf{x} and fidelity are needed to be separately determined by using different criteria.

On the other hand, information-based approaches to BO (Hennig and Schuler, 2012; Hernández-Lobato et al., 2014), called *entropy search* (ES) and *predictive entropy search* (PES), have been also extended to the multi-fidelity setting (Swersky et al., 2013; Zhang et al., 2017) which can evaluate benefit from observations of any fidelity as a gain of information about the optimal solution. For the optimal solution $\mathbf{x}_* := \operatorname{argmax}_{\mathbf{x}} f(\mathbf{x})$, ES/PES maximize the mutual information between a queried point and \mathbf{x}_* . Unlike local evaluation measures such as EI, the information-based criterion is a measure of global utility which does not require any additional exploit-explore trade-off parameter. However, accurately evaluating the mutual information is notoriously difficult which often requires several assumptions and numerical approximations as we see in Section 4.

In this paper, we propose a novel approach to MFBO based on a variant of ES called *max-value entropy search* (MES). MES considers the information gain for $f_* := \max_{\mathbf{x}} f(\mathbf{x})$ instead of \mathbf{x}_* . Wang and Jegelka (2017) showed that most of the computational processes of MES can be written analytically except for the expectation over the optimal value f_* . This greatly facilitates the computation of the information gain because f_* is in one dimensional space unlike \mathbf{x}_* , and they showed superior performance of MES compared with ES/PES. To design an effective and computationally tractable information-based acquisition function

for MFBO, we extend MES so that observations having different levels of fidelity can be incorporated. We show that the information gain obtained from lower fidelity observations can be simply evaluated in the MES framework. In fact, additional computations compared with MES for usual BO is written analytically except for one dimensional integral, which can be calculated accurately and efficiently by using standard numerical integration techniques. The advantages of our proposed method, called *multi-fidelity max-value entropy search* (MF-MES), are summarized as follows:

- Since the information-based criterion is a global measure of utility, the acquisition function does not have any trade-off parameter needed to be set beforehand.
- The pair of \mathbf{x} and fidelity to be queried can be jointly selected by one common acquisition function.
- Compared with other information-based MFBO, evaluation of the acquisition function is much simpler, and the required numerical approximation is only in one dimensional space.

We empirically demonstrate effectiveness of our approach based on synthetic and benchmark datasets, and further show a real-world application to materials science data.

2 Preliminary

In this section, we first briefly review the standard Gaussian process regression (GPR) model, and describe its multi-fidelity extension which is used throughout the paper.

2.1 Gaussian Process Regression

Suppose that $\mathcal{D}_n = \{(\mathbf{x}_i, y(\mathbf{x}_i))\}_{i=1}^n$ is a set of n training instances, where $\mathbf{x}_i \in \mathbb{R}^d$ and $y(\mathbf{x}_i) \in \mathbb{R}$. The observed output $y(\mathbf{x})$ is assumed to be $y(\mathbf{x}) = f(\mathbf{x}) + \epsilon$ in which a random noise $\epsilon \sim \mathcal{N}(0, \sigma_{\text{noise}}^2)$ is added to the underlying true function $f(\mathbf{x})$. The prior of the function f is the Gaussian process with mean 0 and covariance function $k : \mathbb{R}^d \times \mathbb{R}^d \rightarrow \mathbb{R}$, denoted as

$$f \sim GP(0, k(\mathbf{x}, \mathbf{x}')).$$

Without loss of generality, we can set the prior mean as 0 for brevity. Let $\mathbf{K} \in \mathbb{R}^{n \times n}$ be a kernel matrix in which the (i, j) element is defined by $k(\mathbf{x}_i, \mathbf{x}_j)$, and $\mathbf{y} := (y(\mathbf{x}_1), \dots, y(\mathbf{x}_n))^\top$ be the vector of the observation $y(\mathbf{x}_i)$. The predictive distribution of GPR $f(\mathbf{x}) \mid \mathcal{D}_n \sim \mathcal{N}(\mu(\mathbf{x}), \sigma^2(\mathbf{x}))$ is defined by the following mean function $\mu(\mathbf{x})$ and variance function $\sigma^2(\mathbf{x})$:

$$\begin{aligned} \mu(\mathbf{x}) &= \mathbf{k}_n(\mathbf{x})^\top (\mathbf{K} + \sigma_{\text{noise}}^2 \mathbf{I})^{-1} \mathbf{y}, \\ \sigma^2(\mathbf{x}) &= k(\mathbf{x}, \mathbf{x}) - \mathbf{k}_n(\mathbf{x})^\top (\mathbf{K} + \sigma_{\text{noise}}^2 \mathbf{I})^{-1} \mathbf{k}_n(\mathbf{x}), \end{aligned}$$

where $\mathbf{k}_n(\mathbf{x}) := (k(\mathbf{x}, \mathbf{x}_1), \dots, k(\mathbf{x}, \mathbf{x}_n))^\top$, and \mathbf{I} is the n -dimensional identity matrix.

2.2 Multi-Fidelity Gaussian Process

Suppose that $y^{(1)}(\mathbf{x}), \dots, y^{(M)}(\mathbf{x})$ are the observation values at \mathbf{x} with M different fidelities in which $y^{(M)}(\mathbf{x})$ is the highest fidelity and $y^{(1)}(\mathbf{x})$ is the lowest fidelity. The training data set $\mathcal{D}_n = \{(\mathbf{x}_i, y^{(m_i)}(\mathbf{x}_i), m_i)\}_{i=1}^n$ contains a set of triplets consisting of an input \mathbf{x}_i , fidelity $m_i \in \{1, \dots, M\}$, and an output $y^{(m_i)}(\mathbf{x}_i)$. As a multi-fidelity variant of GPR, we mainly focus on an approach proposed by (Kennedy and O'Hagan, 2000) which we call *multi-fidelity Gaussian process regression* (MF-GPR) in this paper (this model is also known as co-kriging model). MF-GPR has the following two advantageous properties:

- All fidelities are integrated into one common GPR
- Difference among fidelities are adaptively estimated without any additional side information (feature representation) of fidelities

In MF-GPR, each fidelity is represented by GPR $f^{(1)}(\mathbf{x}), \dots, f^{(M)}(\mathbf{x})$, and the observation is modeled as

$$y^{(m)}(\mathbf{x}) = f^{(m)}(\mathbf{x}) + \epsilon, \quad \epsilon \sim \mathcal{N}(0, \sigma_{\text{noise}}^2).$$

Let $f^{(1)} \sim GP(0, k_1(\mathbf{x}, \mathbf{x}'))$ be GPR for fidelity $m = 1$, where $k_1 : \mathbb{R}^{d \times d} \rightarrow \mathbb{R}$ is a kernel function. The output for the fidelity $m = 2, \dots, M$ is recursively defined as

$$f^{(m)}(\mathbf{x}) = f^{(m-1)}(\mathbf{x}) + f_e^{(m-1)}(\mathbf{x}), \quad (1)$$

where, $f_e^{(m-1)} \sim GP(0, k_e(\mathbf{x}, \mathbf{x}'))$ with $k_e : \mathbb{R}^d \times \mathbb{R}^d \rightarrow \mathbb{R}$. The following independence relation is assumed for each $f_e^{(m)}$:

$$f_e^{(m)}(\mathbf{x}) \perp f^{(m')}(\mathbf{x}), \text{ for } m' = 1, \dots, m-1, \quad (2)$$

which means that $f_e^{(m)}$ is independent from fidelities lower than m . Equations (1) and (2) derive a kernel function for a pair of points $(\mathbf{x}, \mathbf{x}')$ in the same fidelity m as follows

$$k_m(\mathbf{x}, \mathbf{x}') := k_1(\mathbf{x}, \mathbf{x}') + (m-1)k_e(\mathbf{x}, \mathbf{x}') \quad (3)$$

and thus, GPR for fidelity m is written as

$$f^{(m)} \sim GP(0, k_m(\mathbf{x}, \mathbf{x}')).$$

Using (1) and (2) again, a kernel function for a pair of training instances $\{(\mathbf{x}_i, y^{(m_i)}(\mathbf{x}_i), m_i), (\mathbf{x}_j, y^{(m_j)}(\mathbf{x}_j), m_j)\}$, which can be from different fidelities, is written as

$$\begin{aligned} k((\mathbf{x}_i, m_i), (\mathbf{x}_j, m_j)) &= \text{cov}\left(f^{(m_i)}(\mathbf{x}_i), f^{(m_j)}(\mathbf{x}_j)\right) \\ &= k_{m_i}(\mathbf{x}_i, \mathbf{x}_j), \end{aligned}$$

where $m_i \leq m_j$ and cov is covariance. Using a kernel matrix $\mathbf{K} \in \mathbb{R}^{n \times n}$ in which the i, j element is defined by $k((\mathbf{x}_i, m_i), (\mathbf{x}_j, m_j))$, GPR for all fidelities $f^{(1)}, \dots, f^{(M)}$ can be integrated into one common GPR by which predictive mean and variance are obtained as

$$\mu^{(m)}(\mathbf{x}) = \mathbf{k}_n^{(m)}(\mathbf{x})^\top (\mathbf{K} + \sigma_{\text{noise}}^2 \mathbf{I})^{-1} \mathbf{y}, \quad (4)$$

$$\begin{aligned} \sigma^{2(m)}(\mathbf{x}) &= k((\mathbf{x}, m), (\mathbf{x}, m)) \\ &\quad - \mathbf{k}_n^{(m)}(\mathbf{x})^\top (\mathbf{K} + \sigma_{\text{noise}}^2 \mathbf{I})^{-1} \mathbf{k}_n^{(m)}(\mathbf{x}), \end{aligned} \quad (5)$$

where $\mathbf{y} = (y_1^{(m_1)}(\mathbf{x}_1), \dots, y_n^{(m_n)}(\mathbf{x}_n))^\top$ and $\mathbf{k}_n^{(m)}(\mathbf{x}) := (k((\mathbf{x}, m), (\mathbf{x}_1, m_1)), \dots, k((\mathbf{x}, m), (\mathbf{x}_n, m_n)))^\top$. For later use, we define $\sigma^{2(mm')}(\mathbf{x})$ as the predictive covariance between (\mathbf{x}, m) and (\mathbf{x}, m') , i.e., covariance for identical \mathbf{x} at different fidelities:

$$\begin{aligned} \sigma^{2(mm')}(\mathbf{x}) &= k((\mathbf{x}, m), (\mathbf{x}, m')) \\ &\quad - \mathbf{k}_n^{(m)}(\mathbf{x})^\top (\mathbf{K} + \sigma_{\text{noise}}^2 \mathbf{I})^{-1} \mathbf{k}_n^{(m')}(\mathbf{x}). \end{aligned} \quad (6)$$

3 Multi-fidelity Bayesian Optimization with Max-value Entropy

We consider applying Bayesian optimization (BO) to the maximization of the highest fidelity function $f^{(M)}(\mathbf{x})$ when M different fidelities $y^{(m)}(\mathbf{x})$ for $m = 1, \dots, M$ are available to querying in an input domain \mathcal{X} . The querying cost is assumed to be known as $\lambda^{(m)}$, where $\lambda^{(1)} \leq \lambda^{(2)} \dots \leq \lambda^{(M)}$. Our goal is to achieve a higher value with smaller total cost of the queryings. We call this problem *multi-fidelity Bayesian optimization* (MFBO). When $M = 1$, MFBO is reduced to the usual black box optimization to which we refer the single fidelity setting, while we call the setting $M \geq 2$ multi-fidelity setting. Hereafter, we use the notation $f_{\mathbf{x}}^{(m)} := f^{(m)}(\mathbf{x})$ for brevity.

To construct an efficient MFBO algorithm, we employ the information-based approach which has been widely used in the single fidelity BO literature and has shown its superior performance. In particular, our approach is inspired by *max-value entropy search* (MES) (Wang and Jegelka, 2017), which considers *information gain* about the optimal value $\max_{\mathbf{x} \in \mathcal{X}} f(\mathbf{x})$ obtained by a querying. In the case of MFBO, we need to consider the information gain for identifying the maximum of the highest fidelity $f_* := \max_{\mathbf{x} \in \mathcal{X}} f^{(M)}(\mathbf{x})$ by observing an arbitrary fidelity observation, meaning that the acquisition function should be a function of \mathbf{x} and m . Suppose that we already have a training data set \mathcal{D}_t and need to determine next \mathbf{x}_{t+1} and m_{t+1} to be queried. Our acquisition function is defined by

$$a(\mathbf{x}, m) := I(f_*; f_{\mathbf{x}}^{(m)}) / \lambda^{(m)}, \quad (7)$$

where I is the mutual information

$$\begin{aligned} I(f_*; f_{\mathbf{x}}^{(m)}) &:= \int p(f_*, f_{\mathbf{x}}^{(m)} \mid \mathbf{x}, \mathcal{D}_t) \\ &\quad \cdot \log \frac{p(f_*, f_{\mathbf{x}}^{(m)} \mid \mathbf{x}, \mathcal{D}_t)}{p(f_* \mid \mathbf{x}, \mathcal{D}_t)p(f_{\mathbf{x}}^{(m)} \mid \mathbf{x}, \mathcal{D}_t)} df_* df_{\mathbf{x}}^{(m)}. \end{aligned} \quad (8)$$

The information-based criterion is particularly useful for MFBO because

- (a) It provides a natural way to evaluate benefit of observing lower fidelity observations, which is sometimes difficult for classical acquisition functions such as expected improvement (EI) . Although some studies extend classical EI to MFBO (Huang et al., 2006; Picheny et al., 2013; Lam et al., 2015), the resulting criteria are heuristic and difficult to be rigorously justified.
- (b) The acquisition function (7) can simultaneously select a pair of \mathbf{x} and m based on one shared criterion, and the selected pair can be clearly interpreted as a pair which achieves the best information gain per unit cost.

Although information-based approaches often result in complicated computations, we show that the calculation of our information gain (8) is quite simple by which reliable evaluation of the acquisition function (7) becomes possible.

3.1 Evaluating Information Gain across Multiple Fidelities

Here, we describe calculation of the mutual information (8). The mutual information can be written as the difference of the entropy:

$$I(f_*; f_{\mathbf{x}}^{(m)} | \mathbf{x}, \mathcal{D}_t) = H(f_{\mathbf{x}}^{(m)} | \mathbf{x}, \mathcal{D}_t) - \mathbb{E}_{p(f_* | \mathbf{x}, \mathcal{D}_t)} [H(f_{\mathbf{x}}^{(m)} | \mathbf{x}, f_*, \mathcal{D}_t)], \quad (9)$$

where $H(\cdot | \cdot)$ is the conditional entropy of $p(\cdot | \cdot)$. The first term in the right hand side can be derived analytically for any fidelity m :

$$H(f_{\mathbf{x}}^{(m)} | \mathbf{x}, \mathcal{D}_t) = \log \left(\sigma^{(m)}(\mathbf{x}) \sqrt{2\pi e} \right). \quad (10)$$

The second term in (9) takes expectation over the maximum f_* . Since an analytical formula is not known for this expectation, we employ Monte Carlo estimation by sampling f_* from the current GPR:

$$\begin{aligned} & \mathbb{E}_{p(f_* | \mathbf{x}, \mathcal{D}_t)} [H(f_{\mathbf{x}}^{(m)} | \mathbf{x}, f_*, \mathcal{D}_t)] \\ & \approx \sum_{f_* \in \mathcal{F}_*} \frac{1}{|\mathcal{F}_*|} H(f_{\mathbf{x}}^{(m)} | \mathbf{x}, f_*, \mathcal{D}_t), \end{aligned} \quad (11)$$

where \mathcal{F}_* is a set of sampled f_* . Note that since this sampling approximation is in one dimensional space, accurate approximation can be expected with a small amount of samples. In Section 3.2, we discuss computational procedures of this sampling. For a given sampled f_* , the entropy of $p(f_{\mathbf{x}}^{(m)} | \mathbf{x}, f_*, \mathcal{D}_t)$ is needed to calculate in (11). Following the existing studies of information-based BO (Hernández-Lobato et al., 2014; Wang and Jegelka, 2017), we regard this conditional distribution as $p(f_{\mathbf{x}}^{(m)} | \mathbf{x}, f_{\mathbf{x}}^{(M)} \leq f_*, \mathcal{D}_t)$, i.e., conditioning only on the given \mathbf{x} rather than for $\forall \mathbf{x} \in \mathcal{X}$.

For any $\zeta \in \mathbb{R}$, define

$$\gamma_{\zeta}^{(m)}(\mathbf{x}) := (\zeta - \mu^{(m)}(\mathbf{x})) / \sigma^{(m)}(\mathbf{x})$$

as the scaling function by $\mu^{(m)}$ and $\sigma^{(m)}$. When $m = M$, the density function $p(f_{\mathbf{x}}^{(m)} | \mathbf{x}, f_{\mathbf{x}}^{(M)} \leq f_*, \mathcal{D}_t)$ is written as a *truncated normal distribution*:

$$p(f_{\mathbf{x}}^{(M)} | \mathbf{x}, f_{\mathbf{x}}^{(M)} \leq f_*, \mathcal{D}_t) = \frac{1}{\sigma^{(M)}(\mathbf{x})} \frac{\phi(\gamma_{f_*}^{(M)}(\mathbf{x}))}{\Phi(\gamma_{f_*}^{(M)}(\mathbf{x}))},$$

where ϕ and Φ are the probability density function and the cumulative density function of the standard normal distribution. The entropy of truncated normal distribution can be analytically represented as follows (Michalowicz, 2014):

$$\begin{aligned} H(f_{\mathbf{x}}^{(M)} | \mathbf{x}, f_{\mathbf{x}}^{(M)} \leq f_*, \mathcal{D}_t) \\ = \log \left(\sqrt{2\pi} e \sigma^{(M)}(\mathbf{x}) \Phi(\gamma_{f_*}^{(M)}(\mathbf{x})) \right) + \frac{\gamma_{f_*}^{(M)}(\mathbf{x}) \phi(\gamma_{f_*}^{(M)}(\mathbf{x}))}{2\Phi(\gamma_{f_*}^{(M)}(\mathbf{x}))}. \end{aligned} \quad (12)$$

Next, we consider the case of $m \neq M$. Unlike the case of $m = M$, the density $p(f_{\mathbf{x}}^{(m)} | \mathbf{x}, f_{\mathbf{x}}^{(M)} \leq f_*, \mathcal{D}_t)$ is not the truncated normal. Using Bayes' theorem, we obtain

$$\begin{aligned} p(f_{\mathbf{x}}^{(m)} | \mathbf{x}, f_{\mathbf{x}}^{(M)} \leq f_*, \mathcal{D}_t) \\ = \frac{p(f_{\mathbf{x}}^{(M)} \leq f_* | f_{\mathbf{x}}^{(m)}, \mathbf{x}, \mathcal{D}_t) p(f_{\mathbf{x}}^{(m)} | \mathbf{x}, \mathcal{D}_t)}{p(f_{\mathbf{x}}^{(M)} \leq f_* | \mathbf{x}, \mathcal{D}_t)}. \end{aligned} \quad (13)$$

The densities $p(f_{\mathbf{x}}^{(m)} | \mathbf{x}, \mathcal{D}_t)$ and $p(f_{\mathbf{x}}^{(M)} \leq f_* | \mathbf{x}, \mathcal{D}_t)$ are directly obtained from the predictive distribution:

$$\begin{aligned} p(f_{\mathbf{x}}^{(m)} | \mathbf{x}, \mathcal{D}_t) &= \frac{1}{\sigma^{(m)}(\mathbf{x})} \phi(\gamma_{f_*}^{(m)}), \\ p(f_{\mathbf{x}}^{(M)} \leq f_* | \mathbf{x}, \mathcal{D}_t) &= \Phi(\gamma_{f_*}^{(M)}). \end{aligned} \quad (14)$$

Remaining $p(f_{\mathbf{x}}^{(M)} \leq f_* | f_{\mathbf{x}}^{(m)}, \mathbf{x}, \mathcal{D}_t)$ is based on the distribution of $f_{\mathbf{x}}^{(M)}$ after additionally observing $f_{\mathbf{x}}^{(m)}$. Since MF-GPR represents all fidelities as one common GPR, the joint marginal distribution $p(f_{\mathbf{x}}^{(M)}, f_{\mathbf{x}}^{(m)} | \mathbf{x}, \mathcal{D}_t)$ is written as

$$\begin{aligned} \begin{bmatrix} f_{\mathbf{x}}^{(m)} \\ f_{\mathbf{x}}^{(M)} \end{bmatrix} | \mathbf{x}, \mathcal{D}_t \\ \sim \mathcal{N} \left(\begin{bmatrix} \mu^{(m)}(\mathbf{x}) \\ \mu^{(M)}(\mathbf{x}) \end{bmatrix}, \begin{bmatrix} \sigma^{2(m)}(\mathbf{x}) & \sigma^{2(mM)}(\mathbf{x}) \\ \sigma^{2(mM)}(\mathbf{x}) & \sigma^{2(M)}(\mathbf{x}) \end{bmatrix} \right), \end{aligned} \quad (15)$$

where each element in the mean and the covariance is from the posterior distribution of MF-GPR (4), (5) and (6). From this distribution, we obtain $p(f_{\mathbf{x}}^{(M)} | f_{\mathbf{x}}^{(m)}, \mathbf{x}, \mathcal{D}_t)$ as

$$f_{\mathbf{x}}^{(M)} | f_{\mathbf{x}}^{(m)}, \mathbf{x}, \mathcal{D}_t \sim \mathcal{N}(u(\mathbf{x}), s^2(\mathbf{x})),$$

where

$$\begin{aligned} u(\mathbf{x}) &= \frac{\sigma^{2(mM)}(\mathbf{x})(f_{\mathbf{x}}^{(m)} - \mu^{(m)}(\mathbf{x}))}{\sigma^{2(m)}(\mathbf{x})} + \mu^{(M)}(\mathbf{x}), \\ s^2(\mathbf{x}) &= \sigma^{2(M)}(\mathbf{x}) - (\sigma^{2(mM)}(\mathbf{x}))^2 / \sigma^{2(m)}(\mathbf{x}). \end{aligned}$$

Thus, $p(f_{\mathbf{x}}^{(M)} \leq f_* \mid f_{\mathbf{x}}^{(m)}, \mathbf{x}, \mathcal{D}_t)$ is written as the cumulative distribution of this Gaussian:

$$p(f_{\mathbf{x}}^{(M)} \leq f_* \mid f_{\mathbf{x}}^{(m)}, \mathbf{x}, \mathcal{D}_t) = \Phi(\gamma'_{f_*}(\mathbf{x})), \quad (16)$$

where, $\gamma'_{f_*}(\mathbf{x}) := (f_* - u(\mathbf{x}))/s(\mathbf{x})$. Substituting (14) and (16) into (13), the entropy is obtained as

$$\begin{aligned} H(f_{\mathbf{x}}^{(m)} \mid \mathbf{x}, f_{\mathbf{x}}^{(M)} \leq f_*, \mathcal{D}_t) \\ = - \int Z \Phi(\gamma'_{f_*}(\mathbf{x})) \phi(\gamma_{f_{\mathbf{x}}^{(m)}}^{(m)}(\mathbf{x})) \\ \cdot \log \left(Z \Phi(\gamma'_{f_*}(\mathbf{x})) \phi(\gamma_{f_{\mathbf{x}}^{(m)}}^{(m)}(\mathbf{x})) \right) \mathrm{d}f_{\mathbf{x}}^{(m)}, \end{aligned} \quad (17)$$

where $Z := 1/\sigma^{(m)}(\mathbf{x})\Phi(\gamma_{f_*}^{(M)}(\mathbf{x}))$, is a constant which does not depend on the integrated variable $f_{\mathbf{x}}^{(m)}$. We calculate the integral in (17) by using numerical integration (e.g., quadrature). Since the integral is only over one dimensional variable $f_{\mathbf{x}}^{(m)}$, numerical integration can provide precise approximation.

3.2 Computations

Algorithm 1 shows the procedure of our proposed method called *Multi-fidelity max-value entropy search* (MF-MES). As the first step in the every iteration, a set of max values \mathcal{F}_* are sampled from $p(f_* \mid \mathcal{D}_t)$. There are several approaches to sampling the max value. Wang and Jegelka (2017) show efficient approximation by Gumbel distribution and random feature map based sampling from the GPR posterior. Gumbel distribution is widely known in extreme value theory (Gumbel, 1958) as one of generalized extreme value distributions. By fitting Gumbel distribution parameters to current GPR, Wang and Jegelka (2017) generate the max values from the fitted Gumbel distribution. Random feature map (Rahimi and Recht, 2008) approximates GPR based on a set of pre-defined basis functions $\phi(\mathbf{x}) \in \mathbb{R}^D$: $f_{\mathbf{x}}^{(M)} \approx \mathbf{a}^\top \phi(\mathbf{x})$, where $\mathbf{a} \in \mathbb{R}^D$. By generating the parameter \mathbf{a} from the posterior, the maximum can be taken from the approximate $f_{\mathbf{x}}^{(M)}$. For further detail of these two approaches, see (Wang and Jegelka, 2017), in which it is also shown that MES is empirically robust with respect to this sampling, and theoretically, they showed that the regret bound can be derived even only for one sample of f_* .

Once, \mathcal{F}_* is generated, the acquisition function calculation can be analytically performed except for one dimensional numerical integration. Although most complicated process in the algorithm is the calculation of (17) shown in line 16 of Algorithm 1, this is also quite simple in practice as described below. For given f_* and the two dimensional marginal predictive distribution (15), the integral of (17) can be computed by $O(1)$ if we regard computational complexity of one dimensional numerical integration as $O(1)$. Further, since (15) does not depend on sampled f_* , it is not required to re-calculate the two dimensional predictive distribution (15) for each one of sampled f_* .

Although we use $I(f_*; f_{\mathbf{x}}^{(m)})$ as the information gain throughout the paper, using $I(f_*; y^{(m)}(\mathbf{x}))$, in which noisy observation $y^{(m)}(\mathbf{x})$ is contained, would be another possible definition. We employed $I(f_*; f_{\mathbf{x}}^{(m)})$ just for notational simplicity, and $I(f_*; y^{(m)}(\mathbf{x}))$ is also possible to use with the almost same computational procedure (for details, see supplementary appendix A).

Algorithm 1 Multi-fidelity Bayesian Optimization with Max-value Entropy Search

```
1: function MF-MES( $\mathcal{D}_0, M, \mathcal{X}, \lambda^{(1)}, \dots, \lambda^{(M)}$ )
2:   for  $t = 0, \dots, T$  do
3:     Generate  $\mathcal{F}_*$  based on current  $f^{(M)}(\mathbf{x})$ 
4:      $(\mathbf{x}_{t+1}, m_{t+1}) \leftarrow \operatorname{argmax}_{\mathbf{x} \in \mathcal{X}, m=1, \dots, M}$ 
       INFOGAIN( $\mathbf{x}, m, \mathcal{F}_*, \mathcal{D}_t$ ) /  $\lambda^{(m)}$ 
5:      $\mathcal{D}_{t+1} \leftarrow \mathcal{D}_t \cup (\mathbf{x}_t, y^{(m_{t+1})}(\mathbf{x}_{t+1}), m_{t+1})$ 
6:   end for
7: end function
8: function INFOGAIN( $\mathbf{x}, m, \mathcal{F}_*, \mathcal{D}_t$ )
9:   Calculate  $\mu^{(M)}(\mathbf{x})$  and  $\sigma^{(M)}(\mathbf{x})$ 
10:  if  $m = M$  then
11:    Set  $H_0 \leftarrow H(f_{\mathbf{x}}^{(M)} \mid \mathbf{x}, \mathcal{D}_t)$  by using (10)
12:    Set  $H_1 \leftarrow$ 
        $\sum_{f_* \in \mathcal{F}_*} \frac{1}{|\mathcal{F}_*|} H(f_{\mathbf{x}}^{(M)} \mid \mathbf{x}, f_{\mathbf{x}}^{(M)} \leq f_*, \mathcal{D}_t)$ 
       by using (12)
13:  else
14:    Calculate  $\mu^{(m)}(\mathbf{x}), \sigma^{(m)}(\mathbf{x})$ , and  $\sigma^{2(mM)}(\mathbf{x})$ 
15:    Set  $H_0 \leftarrow H(f_{\mathbf{x}}^{(m)} \mid \mathbf{x}, \mathcal{D}_t)$  by using (10)
16:    Set  $H_1 \leftarrow$ 
        $\sum_{f_* \in \mathcal{F}_*} \frac{1}{|\mathcal{F}_*|} H(f_{\mathbf{x}}^{(m)} \mid \mathbf{x}, f_{\mathbf{x}}^{(M)} \leq f_*, \mathcal{D}_t)$ 
       by using (17)
17:  end if
18:  Return  $H_0 - H_1$ 
19: end function
```

3.3 Extension to General Fidelity Space

Our proposed method is applicable to the case that the fidelity is defined as a point of a fidelity space \mathcal{Z} instead of the discrete fidelity level $1, \dots, M$ (Kandasamy et al., 2017). Let $f_{\mathbf{x}}^{(\mathbf{z})}$ be the predictive distribution for the fidelity $\mathbf{z} \in \mathcal{Z}$. The goal is to solve $\max_{\mathbf{x} \in \mathcal{X}} f_{\mathbf{x}}^{(\mathbf{z}_*)}$, where $\mathbf{z}_* \in \mathcal{Z}$ is the highest fidelity to be optimized. For example, in the neural network hyper-parameter optimization, \mathcal{Z} can be a two dimensional space defined by the number of training data and the number of training iterations.

In this case, our acquisition function (8) is extended to

$$a(\mathbf{x}, \mathbf{z}) := I(f_*; f_{\mathbf{x}}^{(\mathbf{z})}) / \lambda^{(\mathbf{z})}, \quad (18)$$

where $f_* := \max_{\mathbf{x} \in \mathcal{X}} f_{\mathbf{x}}^{(\mathbf{z}_*)}$ in this case, and $\lambda^{(\mathbf{z})}$ is known cost for $\mathbf{z} \in \mathcal{Z}$. As with (Kandasamy et al., 2017),

we represent the output $f_{\mathbf{x}}^{(\mathbf{z})}$ as a Gaussian process on the direct product space $\mathcal{X} \times \mathcal{Z}$. Suppose that the observed training data set is written as $\mathcal{D}_n = \{(\mathbf{x}_i, y^{(\mathbf{z}_i)}(\mathbf{x}_i), \mathbf{z}_i)\}_{i=1}^n$, where $y^{(\mathbf{z}_i)}(\mathbf{x}_i)$ is an observation of \mathbf{x}_i at the fidelity \mathbf{z}_i . A standard approach to defining a kernel on the joint space $\mathcal{X} \times \mathcal{Z}$ is to use the product form $k((\mathbf{x}_i, \mathbf{z}_i), (\mathbf{x}_j, \mathbf{z}_j)) = k_x(\mathbf{x}_i, \mathbf{x}_j) k_z(\mathbf{z}_i, \mathbf{z}_j)$, where $k_x : \mathcal{X} \times \mathcal{X} \rightarrow \mathbb{R}$ is a kernel for the input space \mathcal{X} , and $k_z : \mathcal{Z} \times \mathcal{Z} \rightarrow \mathbb{R}$ is a kernel for the fidelity space \mathcal{Z} . Based on this kernel, predictive distribution of GPR can be defined for any pair of (\mathbf{x}, \mathbf{z}) , and thus the numerator of (18) can be calculated by using the same approach as $I(f_*; f_{\mathbf{x}}^{(m)})$ which we describe in Section 3.1.

4 Related Work

The entropy based BO was first proposed by (Hennig and Schuler, 2012). They defined an acquisition function by using the negative differential entropy over $p(\mathbf{x}_*)$, where $\mathbf{x}_* := \operatorname{argmax}_{\mathbf{x}} f(\mathbf{x})$ is the optimal solution:

$$a_{ES}(\mathbf{x}) = H(\mathbf{x}_* | \mathcal{D}_t) - \mathbb{E}_{p(y | \mathcal{D}_t, \mathbf{x})} [H(\mathbf{x}_* | \mathcal{D}_t, \mathbf{x}, y(\mathbf{x}))].$$

This approach, called *entropy search* (ES), can measure the *global* benefit of the decision because the entropy of $p(\mathbf{x}_*)$ evaluates uncertainty of \mathbf{x}_* in the entire input space, while classical probabilistic improvement (PI) and EI are local measurements of utility. Because of this property, the acquisition function of ES is free from any tuning parameter of exploit-explore trade-off, and has shown its superior practical performance. However, exact computation of this acquisition function is infeasible in practice, and many approximations should be performed.

To mitigate computational difficulty of the entropy, *predictive entropy search* (PES) proposed by (Hernández-Lobato et al., 2014) derives an efficient computation based on the following equivalent representation to $a_{ES}(\mathbf{x})$:

$$a_{PES}(\mathbf{x}) = H(y(\mathbf{x}) | \mathcal{D}_t, \mathbf{x}) - \mathbb{E}_{p(\mathbf{x}_* | \mathcal{D}_t)} [H(y(\mathbf{x}) | \mathcal{D}_t, \mathbf{x}, \mathbf{x}_*)].$$

However, PES is still quite difficult to compute mainly because of i) the expectation over $p(\mathbf{x}_* | \mathcal{D}_t)$, and ii) the entropy of $p(y(\mathbf{x}) | \mathcal{D}_t, \mathbf{x}, \mathbf{x}_*)$. For i), since $p(\mathbf{x}_* | \mathcal{D}_t)$ is analytically intractable, sampling approximation is necessary though the dimension of \mathbf{x}_* can be high. For ii), after introducing several assumptions to simplify the density, approximations such as expectation propagation (Minka, 2001) are further necessary. On the other hand, (Hoffman and Ghahramani, 2015; Wang and Jegelka, 2017) proposed using the information gain for f_* instead of \mathbf{x}_* . In particular, MES (Wang and Jegelka, 2017) efficiently calculates the entropy by representing a condition distribution of $f(\mathbf{x})$ given f_* as a truncated normal distribution as we follow the same approach in (12). Our proposed method is a multi-fidelity extension of MES. As we see in Section 3.1, for the information gain from a lower fidelity, the truncated normal approach is not applicable anymore because lower fidelity functions $f_{\mathbf{x}}^{(m)}$ for $m = 1, \dots, M - 1$ are not truncated for given f_* . We already show that this computation can be simplified in such a way that additional computations compared with

single fidelity MES can be written analytically except for one dimensional integral which is easy to calculate accurately by using standard numerical integration techniques. For further acceleration of MES, Ru et al. (2018) proposed approximating the density of f_* and f given f_* by normal distributions, but reliability of these approximations are not clearly understood, and thus we do not employ in this paper.

Multi-fidelity extension of BO has been widely studied. For example, (Huang et al., 2006; Lam et al., 2015; Picheny et al., 2013) extended standard EI to the multi-fidelity setting. As with the usual EI, these are local measures of utility unlike our information based approach. *Gaussian process upper confidence bound* (GP-UCB) (Srinivas et al., 2010) is a popular approach in the single fidelity setting, and some studies proposed its multi-fidelity extensions. Kandasamy et al. (2016) proposed multi-fidelity GP-UCB for discrete fidelity $m = 1, \dots, M$, and further, Kandasamy et al. (2017) proposed a similar UCB-based approach for general fidelity space \mathbf{z} . However, the UCB criterion has a trade-off parameter which balances exploit-exploration. In practice, this parameter needs to be carefully selected to achieve good performance. Another approach recently proposed in (Sen et al., 2018) is a multi-fidelity extension of a hierarchical space partitioning (Bubeck et al., 2011). However, this method assumes that the approximation error can be represented as a known function form of cost, and further, they associate fidelity with the depth of hierarchical tree, but the appropriateness of a specific choice of a pair of a point \mathbf{x} and fidelity m is difficult to interpret.

Information-based BO has also been studied for the multi-fidelity setting, including ES-based (Swersky et al., 2013; Klein et al., 2017) and PES-based (Zhang et al., 2017; McLeod et al., 2018) methods. However, these methods inherit the computational difficulty of the original ES and PES, and further, additional assumptions about inter-fidelity differences are required in the case of (Zhang et al., 2017). Song et al. (2018) proposed another information-based approach. They evaluate information from a lower fidelity function by the mutual information $I(f^{(M)}; f^{(m)}(\mathbf{x}))$ which is the information gain for the entire highest fidelity function $f^{(M)}$. Since this information can not select a point among the highest fidelity function, separate phases of the low-fidelity exploration and the highest fidelity optimization are necessary. The transition of these phases are controlled by a hyper-parameter which is necessary to set appropriately beforehand. Another approach which incorporates global utility would be knowledge gradient approaches (Poloczek et al., 2017; Wu and Frazier, 2017). This approach evaluates the max gain of predictive mean $\max_{\mathbf{x} \in \mathcal{X}} \mu^{(M)}(\mathbf{x})$. However, the acquisition function evaluation requires the expected value of the maximum of the mean function $\mathbb{E}[\max_{\mathbf{x}' \in \mathcal{X}} \mu^{(M)}(\mathbf{x}')]$ after adding $y^{(m)}(\mathbf{x})$ into training set. Thus, the maximization of the acquisition function becomes a nested optimization which is computationally quite expensive.

Since our MF-MES is based on information gain, the advantages of the ES-based approach are succeeded. The acquisition function is global measure of utility in a sense of information gain for f_* , and thus no exploit-exploration trade-off parameter is necessary. This property is also useful for selecting fidelity m because the information gain per unit cost provides a seamless evaluation measure over different fidelity observations. Further, we show that computations of MF-MES is quite simple. This is beneficial for both

of the accuracy and computational efficiency of the acquisition function. To fully exploit lower fidelity information, computations of the acquisition function should not be a bottleneck.

5 Experiments

We evaluate effectiveness of MF-MES by using a synthetic dataset, benchmark functions, and a real-world dataset from materials science. For comparison, we used MF-SKO (Huang et al., 2006), multi-fidelity GP-UCB (MFGP-UCB) (Kandasamy et al., 2016), Bayesian optimization with continuous approximations (BOCA) (Kandasamy et al., 2017), and multi-fidelity PES (MF-PES) (Zhang et al., 2017). We also evaluated single fidelity MES which applied to the highest fidelity function $f^{(M)}(\mathbf{x})$ to see the effect of MFBO. For the kernel function in the all methods, we employed the standard Gaussian kernel $k(\mathbf{x}, \mathbf{x}') = \exp(-\|\mathbf{x} - \mathbf{x}'\|_2^2 / (2\sigma^2))$. MF-SKO, MF-PES, and MF-MES used the same MF-GPR model in which the kernel function (3) was set as $k_1(\mathbf{x}, \mathbf{x}') = k(\mathbf{x}, \mathbf{x}')$ and $k_e(\mathbf{x}, \mathbf{x}') = \sigma_e k(\mathbf{x}, \mathbf{x}')$, where σ_e is a hyperparameter which is fixed as $\sigma_e = 0.1$ throughout all the experiments. For the sampling of f_* in MES and MF-MES, Gumbel distribution approximation shown by (Wang and Jegelka, 2017) was used, and we sampled 10 f_* s at every iteration. In the case of MF-PES, \mathbf{x}_* was sampled 10 times through random feature map as suggested by (Hernández-Lobato et al., 2014). The initial training data were set by randomly selected 10 lowest fidelity observations except for MES which uses the highest fidelity function only. The GPR kernel hyperparameter σ was optimized by the marginal likelihood maximization at every 5 iterations. To avoid undesired bias from the acquisition function maximization algorithm, the fixed discrete set \mathcal{X} was generated beforehand as candidate points, and the exact maximum of each acquisition function was selected as the next query. All experiments were performed 10 times with different initial training sets. To evaluate performance, we employed *inference regret* (IR). IR is defined by $R_t := \max_{\mathbf{x} \in \mathcal{X}} f^{(M)}(\mathbf{x}) - f^{(M)}(\hat{\mathbf{x}}_t)$, where $\hat{\mathbf{x}}_t := \operatorname{argmax}_{\mathbf{x} \in \mathcal{X}} \mu^{(M)}(\mathbf{x})$ which is considered as the recommendation from each method at iteration t (We also show all the results with *simple regret* in supplementary appendix E). The other detailed experimental settings are shown in supplementary appendix B

5.1 Synthetic Dataset

We generated a three dimensional synthetic multi-fidelity dataset by sampling from the MF-GPR model. The input $\mathbf{x} \in \mathcal{X}$ was from 5000 points of uniform distribution in $[0, 1]^3$. For data generating MF-GPR, the Gaussian kernel width parameter is set as $1/(2\sigma^2) = 0.05d_{\text{mean}}^2$, where d_{mean} is the mean of distances in the candidate set \mathcal{X} . The objective function has many local maximums. The number of fidelity levels was set as $M = 3$ and the coefficient of k_e was $\sigma_e = 0.1$. The cost is defined as $\lambda^{(1)} = 1$, $\lambda^{(2)} = 3$, and $\lambda^{(3)} = 10$.

We here compared three information theoretic approaches, i.e., MES, MF-PES, and MF-MES, based on IR. The result is shown in Figure 1. Since MES initially took the 10 highest fidelity points, the cost started from 100 while the other two methods started from cost 10. First, we clearly see that two MFBO

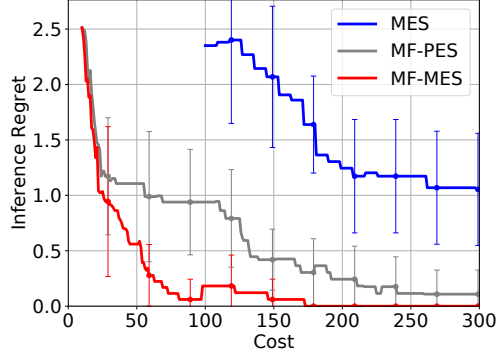


Figure 1: Inference regret on the three dimensional synthetic dataset. The average and standard deviation of 10 runs are shown.

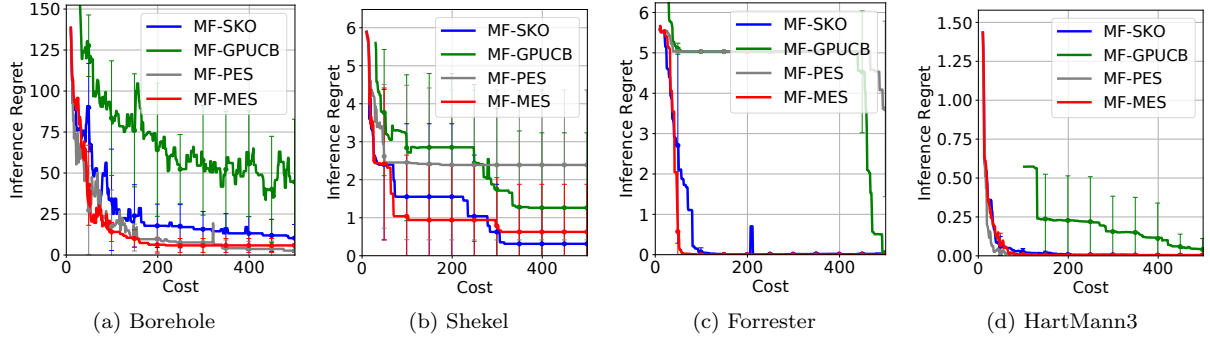


Figure 2: Inference regret on the benchmark functions. The average and standard deviation of 10 runs are shown.

methods rapidly decrease IR compared with the single fidelity MES, meaning that lower fidelity observations successfully accelerated the optimization process. We also see that compared with MF-PES, MF-MES was much faster and its standard deviation was small at the later half of the optimization which would be resulted from more stable evaluation of entropy.

5.2 Benchmark Functions

We used four benchmark functions called Borehole ($d = 8, M = 2$), Shekel ($d = 4, M = 2$), Forrester ($d = 1, M = 2$), and HartMann3 ($d = 3, M = 3$), for which definition can be found in (Surjanovic and Bingham, 2013). For the functions with $M = 2$, we set $\lambda^{(1)} = 1$ and $\lambda^{(2)} = 5$, and for functions with $M = 3$, we set $\lambda^{(1)} = 1$, $\lambda^{(2)} = 3$ and $\lambda^{(3)} = 5$. For Borehole and Forrester, surrogate functions which can be used as lower fidelity functions are available at (Surjanovic and Bingham, 2013). For the other two functions, we created lower fidelity functions by slightly changing coefficients in the original functions (See supplementary appendix C for detail). In Forrester, the input x was set as the equally spaced 200 grid points in $[0, 1]$. For

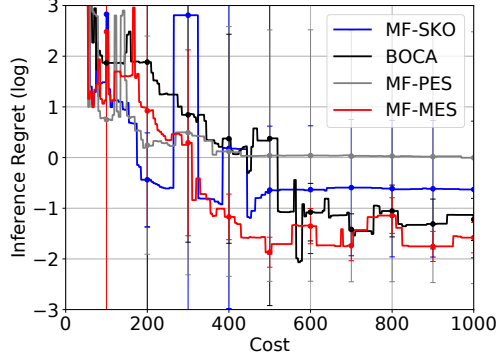


Figure 3: Inference regret on the materials dataset. The average and standard deviation of 10 runs are shown.

the other functions, 50000 points are randomly selected from the uniform distribution as the candidate set \mathcal{X} .

The results are shown in Figure 2. We see that for all the four datasets, MF-MES rapidly decreased IR. MF-GPUCB were relatively slow in these results. A main reason would be that it estimates GPR separately for each fidelity unlike the other MF-GRP based methods, and the setting of trade-off parameter, for which we used the setting (Kandasamy et al., 2016) suggested, might have effect on accuracy. In Shekel and HartMann3, MF-SKO showed comparable performance with MF-MES. Regardless of its weak theoretical justification, MF-SKO showed empirically stable results in our experiments though for the other two datasets, MF-MES outperformed MF-SKO. In Borehole and HartMann3, MF-PES showed comparable performance with MF-MES. However, in the other two datasets, the convergence of MF-PES was quite slow. This unstability can come from difficulty in entropy computations, and sensitivity to sampled \mathbf{x}_* . Using the Forrester dataset, which is simple one dimensional function, we observed detailed behavior of MF-PES in supplementary appendix D.

5.3 Application to Materials Science Data

As an example of practical application, we applied our method to the parameter optimization of computational simulation model in materials science. There is a computational model (Tsukada et al., 2014) that predicts equilibrium shape of precipitates in the α -Mg phase when material parameters are given. Here, we estimate two material parameters (lattice mismatch and interface energy between the α -Mg and precipitate phases) from experimental data on precipitate shape measured by using transmission electron microscopy (TEM) (Bhattacharjee et al., 2013). The objective function is the discrepancy between precipitate shape predicted by the computational model and one measured by TEM. The cost of objective function evaluation depends on the prediction accuracy of the computational model; lower-, middle- and higher-fidelity functions take five minutes, ten minutes and sixty minutes to evaluate, respectively, and thus we set $\lambda^{(1)} = 5$,

$\lambda^{(2)} = 10$, and $\lambda^{(3)} = 60$. Each fidelity has 62500 candidate points. In this dataset, we used MF-SKO, BOCA, MF-PES for comparison, and in BOCA, the computational time 5, 10, and 60 were regarded as the elements of the fidelity space \mathcal{Z} .

The result is shown in Figure 3. Since this dataset contains noisy observations, the lines sometimes fluctuate. MF-PES and MF-SKO first decreased the regret, but the decrease stagnated. BOCA showed reasonably good performance, but the decrease was slightly slower than the other methods at the beginning of the optimization. Among these four methods, we see that MF-MES most stably decreased the regret in this application task.

6 Conclusion

We proposed a novel information theoretic approach to multi-fidelity Bayesian optimization (MFBO). We defined an acquisition function based on the information gain about the optimal value f_* of the highest fidelity function. Unlike local utility measures, the information based acquisition function is free from the trade-off parameter of exploit and exploration. Further, we show that our method called MF-MES (MFBO with max-value entropy search) can be reduced to simple computations in which the sampling approximation and the numerical integration are required only for one dimensional space. This greatly facilitates reliable evaluation of the acquisition function compared with other information-based MFBO methods which are plagued by computational difficulties of the information gain of $p(\mathbf{x}_*)$. We demonstrated effectiveness of MF-MES by using a synthetic dataset, benchmark functions, and a real-world materials science data.

Acknowledgements

This work was supported by MEXT KAKENHI to I.T. (16H06538, 17H00758), M.K. (16H06538, 17H04694) and M.S (16H02866); from JST CREST awarded to I.T. (JPMJCR1302, JPMJCR1502) and PRESTO awarded to M.K. (JPMJPR15N2), M.S (JPMJPR16N6) and Y.T (JPMJPR15NB); from the MI2I project of the Support Program for Starting Up Innovation Hub from JST awarded to I.T., and M.K.; and from RIKEN Center for AIP awarded to M.S. and I.T.

References

- Bhattacharjee, T., Mendis, C., Oh-ishi, K., Ohkubo, T., and Hono, K. (2013). The effect of ag and ca additions on the age hardening response of mgzn alloys. *Materials Science and Engineering: A*, 575:231 – 240.
- Bubeck, S., Munos, R., Stoltz, G., and Szepesvári, C. (2011). X-armed bandits. *Journal of Machine Learning Research*, 12:1655–1695.
- Gumbel, E. J. (1958). *Statistics of Extremes*. Columbia University Press.
- Hennig, P. and Schuler, C. J. (2012). Entropy search for information-efficient global optimization. *Journal of Machine Learning Research*, 13:1809–1837.
- Hernández-Lobato, J. M., Hoffman, M. W., and Ghahramani, Z. (2014). Predictive entropy search for efficient global optimization of black-box functions. In *Advances in Neural Information Processing Systems 27*, pages 918–926. Curran Associates, Inc.
- Hoffman, M. W. and Ghahramani, Z. (2015). Output-space predictive entropy search for flexible global optimization. In *NIPS Workshop on Bayesian Optimization*.
- Huang, D., Allen, T., Notz, W., and Miler, R. (2006). Sequential kriging optimization using multiple-fidelity evaluations. *Structural and Multidisciplinary Optimization*, 32(5):369–382.
- Kandasamy, K., Dasarathy, G., Oliva, J., Schneider, J., and Póczos, B. (2016). Gaussian process bandit optimisation with multi-fidelity evaluations. In *Advances in Neural Information Processing Systems 29*, pages 1000–1008. Curran Associates, Inc.
- Kandasamy, K., Dasarathy, G., Schneider, J., and Póczos, B. (2017). Multi-fidelity Bayesian optimisation with continuous approximations. In *Proceedings of the 34th International Conference on Machine Learning*, pages 1799–1808.
- Kennedy, M. C. and O’Hagan, A. (2000). Predicting the output from a complex computer code when fast approximations are available. *Biometrika*, 87(1):1–13.
- Klein, A., Falkner, S., Bartels, S., Hennig, P., and Hutter, F. (2017). Fast Bayesian optimization of machine learning hyperparameters on large datasets. In *Proceedings of the 20th International Conference on Artificial Intelligence and Statistics*, volume 54, pages 528–536. PMLR.
- Lam, R., Allaire, D. L., and Willcox, K. E. (2015). Multifidelity optimization using statistical surrogate modeling for non-hierarchical information sources. In *Proceedings of the 56th AIAA/ASCE/AHS/ASC Structures, Structural Dynamics, and Materials Conference*, page 0143. American Institute of Aeronautics and Astronautics.

- McLeod, M., Osborne, M. A., and Roberts, S. J. (2018). Practical Bayesian optimization for variable cost objectives. *arXiv:1703.04335*.
- Michalowicz, J. (2014). *Handbook of Differential Entropy*. Chapman and Hall/CRC, New York.
- Minka, T. P. (2001). Expectation propagation for approximate Bayesian inference. In *Proceedings of the 17th Conference in Uncertainty in Artificial Intelligence*, pages 362–369. Morgan Kaufmann Publishers Inc.
- Picheny, V., Ginsbourger, D., Richet, Y., and Caplin, G. (2013). Quantile-based optimization of noisy computer experiments with tunable precision. *Technometrics*, 55(1):2–13.
- Poloczek, M., Wang, J., and Frazier, P. I. (2017). Multi-information source optimization. In *Advances in Neural Information Processing Systems 30*, pages 4288–4298. Curran Associates, Inc.
- Rahimi, A. and Recht, B. (2008). Random features for large-scale kernel machines. In *Advances in Neural Information Processing Systems 20*, pages 1177–1184. Curran Associates, Inc.
- Ramprasad, R., Batra, R., Pilia, G., Mannodi-Kanakkithodi, A., and Kim, C. (2017). Machine learning in materials informatics: recent applications and prospects. *npj Computational Materials*, 3(54).
- Ru, B., Osborne, M. A., McLeod, M., and Granzio, D. (2018). Fast information-theoretic Bayesian optimisation. In *Proceedings of the 35th International Conference on Machine Learning*, volume 80, pages 4384–4392. PMLR.
- Sen, R., Kandasamy, K., and Shakkottai, S. (2018). Multi-fidelity black-box optimization with hierarchical partitions. In *Proceedings of the 35th International Conference on Machine Learning*, volume 80, pages 4538–4547. PMLR.
- Snoek, J., Larochelle, H., and Adams, R. P. (2012). Practical bayesian optimization of machine learning algorithms. In *Advances in Neural Information Processing Systems 25*, pages 2951–2959. Curran Associates, Inc.
- Song, J., Chen, Y., and Yue, Y. (2018). A general framework for multi-fidelity Bayesian optimization with gaussian processes. *arXiv:1811.00755*.
- Srinivas, N., Krause, A., Kakade, S., and Seeger, M. (2010). Gaussian process optimization in the bandit setting: No regret and experimental design. In *Proceedings of the 27th International Conference on International Conference on Machine Learning*, pages 1015–1022. Omnipress.
- Surjanovic, S. and Bingham, D. (2013). Virtual library of simulation experiments: Test functions and datasets. Retrieved January, 2019, from <http://www.sfu.ca/~ssurjano>.

- Swersky, K., Snoek, J., and Adams, R. P. (2013). Multi-task Bayesian optimization. In *Advances in Neural Information Processing Systems 26*, pages 2004–2012. Curran Associates, Inc.
- Tsukada, Y., Beniya, Y., and Koyama, T. (2014). Equilibrium shape of isolated precipitates in the α -mg phase. *Journal of Alloys and Compounds*, 603:65 – 74.
- Wang, Z. and Jegelka, S. (2017). Max-value entropy search for efficient Bayesian optimization. In *Proceedings of the 34th International Conference on Machine Learning*, volume 70, pages 3627–3635. PMLR.
- Wigley, P. B., Everitt, P. J., van den Hengel, A., Bastian, J. W., Sooriyabandara, M. A., McDonald, G. D., Hardman, K. S., Quinlivan, C. D., Manju, P., Kuhn, C. C. N., Petersen, I. R., Luiten, A. N., Hope, J. J., Robins, N. P., and Hush, M. R. (2016). Fast machine-learning online optimization of ultra-cold-atom experiments. *Scientific Reports*, 6:25890.
- Wu, J. and Frazier, P. (2017). Continuous-fidelity Bayesian optimization with knowledge gradient. In *NIPS Workshop on Bayesian Optimization*.
- Zhang, Y., Hoang, T. N., Low, B. K. H., and Kankanhalli, M. (2017). Information-based multifidelity Bayesian optimization. In *NIPS Workshop on Bayesian Optimization*.

Appendix A Information Gain with Noisy Observation

Here, we describe calculation of the mutual information between f_* and noisy observation $y_{\mathbf{x}}^{(m)}$, where $y_{\mathbf{x}}^{(m)} := y^{(m)}(\mathbf{x})$ in this section. The mutual information can be written as the difference of the entropy:

$$I(f_*; y_{\mathbf{x}}^{(m)} | \mathbf{x}, \mathcal{D}_t) = H(y_{\mathbf{x}}^{(m)} | \mathbf{x}, \mathcal{D}_t) - \mathbb{E}_{p(f_* | \mathbf{x}, \mathcal{D}_t)} [H(y_{\mathbf{x}}^{(m)} | \mathbf{x}, f_*, \mathcal{D}_t)]. \quad (19)$$

The first term in the right hand side is

$$H(y_{\mathbf{x}}^{(m)} | \mathbf{x}, \mathcal{D}_t) = \log \left(\sqrt{2\pi e(\sigma^{2(m)}(\mathbf{x}) + \sigma_{\text{noise}}^2)} \right). \quad (20)$$

Using the sampling approximation of f_* , the second term in (19) is

$$\begin{aligned} & \mathbb{E}_{p(f_* | \mathbf{x}, \mathcal{D}_t)} [H(y_{\mathbf{x}}^{(m)} | \mathbf{x}, f_*, \mathcal{D}_t)] \\ & \approx \sum_{f_* \in \mathcal{F}_*} \frac{1}{|\mathcal{F}_*|} H(y_{\mathbf{x}}^{(m)} | \mathbf{x}, f_*, \mathcal{D}_t). \end{aligned} \quad (21)$$

For any $\zeta \in \mathbb{R}$, define

$$\gamma_{\zeta}^{(m)}(\mathbf{x}) := (\zeta - \mu^{(m)}(\mathbf{x})) / \sigma^{(m)}(\mathbf{x}),$$

and

$$\rho_{\zeta}^{(m)}(\mathbf{x}) := (\zeta - \mu^{(m)}(\mathbf{x})) / \sqrt{\sigma^{2(m)}(\mathbf{x}) + \sigma_{\text{noise}}^2}.$$

In this case, even for the highest fidelity M , the density $p(y_{\mathbf{x}}^{(m)} | \mathbf{x}, f_{\mathbf{x}}^{(M)} \leq f_*, \mathcal{D}_t)$ is not the truncated normal because of the noise term. Using Bayes' theorem, we decompose this density as

$$\begin{aligned} & p(y_{\mathbf{x}}^{(m)} | \mathbf{x}, f_{\mathbf{x}}^{(M)} \leq f_*, \mathcal{D}_t) \\ & = \frac{p(f_{\mathbf{x}}^{(M)} \leq f_* | y_{\mathbf{x}}^{(m)}, \mathbf{x}, \mathcal{D}_t) p(y_{\mathbf{x}}^{(m)} | \mathbf{x}, \mathcal{D}_t)}{p(f_{\mathbf{x}}^{(M)} \leq f_* | \mathbf{x}, \mathcal{D}_t)}. \end{aligned} \quad (22)$$

The densities $p(y_{\mathbf{x}}^{(m)} | \mathbf{x}, \mathcal{D}_t)$ and $p(f_{\mathbf{x}}^{(M)} \leq f_* | \mathbf{x}, \mathcal{D}_t)$ are directly obtained from the predictive distribution:

$$\begin{aligned} p(y_{\mathbf{x}}^{(m)} | \mathbf{x}, \mathcal{D}_t) & = \frac{1}{\sqrt{\sigma^{2(m)}(\mathbf{x}) + \sigma_{\text{noise}}^2}} \phi(\rho_{y_{\mathbf{x}}^{(m)}}^{(m)}), \\ p(f_{\mathbf{x}}^{(M)} \leq f_* | \mathbf{x}, \mathcal{D}_t) & = \Phi(\gamma_{f_*}^{(M)}). \end{aligned} \quad (23)$$

The joint marginal distribution $p(f_{\mathbf{x}}^{(M)}, y_{\mathbf{x}}^{(m)} | \mathbf{x}, \mathcal{D}_t)$ is written as

$$\begin{aligned} & \begin{bmatrix} y_{\mathbf{x}}^{(m)} \\ f_{\mathbf{x}}^{(M)} \end{bmatrix} | \mathbf{x}, \mathcal{D}_t \\ & \sim \mathcal{N} \left(\begin{bmatrix} \mu^{(m)}(\mathbf{x}) \\ \mu^{(M)}(\mathbf{x}) \end{bmatrix}, \begin{bmatrix} \sigma^{2(m)}(\mathbf{x}) + \sigma_{\text{noise}}^2 & \sigma^{2(mM)}(\mathbf{x}) \\ \sigma^{2(mM)}(\mathbf{x}) & \sigma^{2(M)}(\mathbf{x}) \end{bmatrix} \right), \end{aligned}$$

From this distribution, we obtain $p(f_{\mathbf{x}}^{(M)} | y_{\mathbf{x}}^{(m)}, \mathbf{x}, \mathcal{D}_t)$ as

$$f_{\mathbf{x}}^{(M)} | y_{\mathbf{x}}^{(m)}, \mathbf{x}, \mathcal{D}_t \sim \mathcal{N}(u(\mathbf{x}), s^2(\mathbf{x})),$$

where

$$\begin{aligned} u(\mathbf{x}) &= \frac{\sigma^{2(mM)}(\mathbf{x})(y_{\mathbf{x}}^{(m)} - \mu^{(m)}(\mathbf{x}))}{\sigma^{2(m)}(\mathbf{x}) + \sigma_{\text{noise}}^2} + \mu^{(M)}(\mathbf{x}), \\ s^2(\mathbf{x}) &= \sigma^{2(M)}(\mathbf{x}) - \frac{(\sigma^{2(mM)}(\mathbf{x}))^2}{\sigma^{2(m)}(\mathbf{x}) + \sigma_{\text{noise}}^2}. \end{aligned}$$

Thus, $p(f_{\mathbf{x}}^{(M)} \leq f_* | y_{\mathbf{x}}^{(m)}, \mathbf{x}, \mathcal{D}_t)$ is written as the cumulative distribution of this Gaussian:

$$p(f_{\mathbf{x}}^{(M)} \leq f_* | y_{\mathbf{x}}^{(m)}, \mathbf{x}, \mathcal{D}_t) = \Phi(\gamma'_{f_*}(\mathbf{x})), \quad (24)$$

where, $\gamma'_{f_*}(\mathbf{x}) := (f_* - u(\mathbf{x}))/s(\mathbf{x})$. Using (13), (14) and (16), the entropy is obtained as

$$\begin{aligned} H(y_{\mathbf{x}}^{(m)} | \mathbf{x}, f_{\mathbf{x}}^{(M)} \leq f_*, \mathcal{D}_t) \\ = - \int Z \Phi(\gamma'_{f_*}(\mathbf{x})) \phi(\rho_{y_{\mathbf{x}}^{(m)}}^{(m)}(\mathbf{x})) \\ \cdot \log \left(Z \Phi(\gamma'_{f_*}(\mathbf{x})) \phi(\rho_{y_{\mathbf{x}}^{(m)}}^{(m)}(\mathbf{x})) \right) dy_{\mathbf{x}}^{(m)}, \end{aligned} \quad (25)$$

where $Z := 1/\sqrt{\sigma^{2(m)}(\mathbf{x}) + \sigma_{\text{noise}}^2} \Phi(\gamma_{f_*}^{(M)}(\mathbf{x}))$. The integral in (25) can be calculated by using numerical integration in the same way as (17).

Using $I(f_*; y_{\mathbf{x}}^{(m)})$ instead of $I(f_*; f_{\mathbf{x}}^{(m)})$ would be more natural when the observations are assumed to contain the large observation noise σ_{noise} , but in practice, difference of these two formulations would not largely effect on performance of BO when σ_{noise} is small.

Appendix B Other Experimental Settings

We here describe the other experimental settings.

- The marginal likelihood maximization for the Gaussian kernel width σ was performed by the grid search from $[0.01L, 10L]$, where L is a value determined by so-called median heuristics (taking median of distance values in \mathcal{X}).
- The noise term σ_{noise} is fixed as 10^{-3} for GPR in all the methods.
- The number of basis D in random feature map used in MF-PES was 100.
- The kernel function $k(\mathbf{z}, \mathbf{z}')$ on the fidelity space of BOCA was also the Gaussian kernel with the median heuristics in the fidelity space.

Appendix C Settings of Benchmark Functions

Shekel function The shekel function is defined as

$$f(\mathbf{x}) = - \sum_{i=1}^k \left(\sum_{j=1}^4 (x_j - C_{ji})^2 + \beta_i \right)^{-1}$$

where C_{ji} for $j = 1, \dots, 4$ and $i = 1, \dots, k$, and β_i for $i = 1, \dots, m$ are constant parameters for which we used values shown in (Surjanovic and Bingham, 2013). We used the function with $k = 10$ as the highest fidelity, and $k = 5$ as the low fidelity function.

HartMann3 function HartMann3 function is defined as

$$f(\mathbf{x}) = - \sum_{i=1}^4 \alpha_i \exp \left(- \sum_{j=1}^3 A_{ij} (x_j - P_{ij})^2 \right)$$

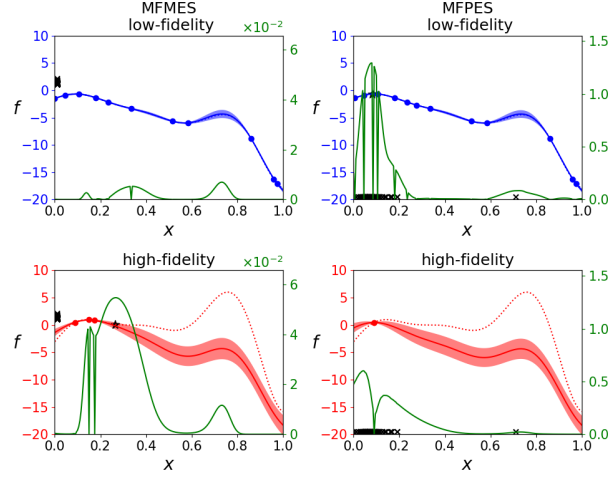
where α_i for $i = 1, \dots, 4$, A_{ij} for $i = 1, \dots, 4$ and $j = 1, \dots, 3$, and P_{ij} for $i, j = 1, \dots, 3$ are constant parameters for which we used values shown in (Surjanovic and Bingham, 2013). The original function is used as the highest fidelity function ($m = M = 3$). For the middle fidelity function ($m = 2$), α_i is replaced by $\alpha_i - 0.1$. For the lowest fidelity function ($m = 1$), α_i is replaced by $\alpha_i - 0.2$.

Appendix D Analysis of Result on Forrester

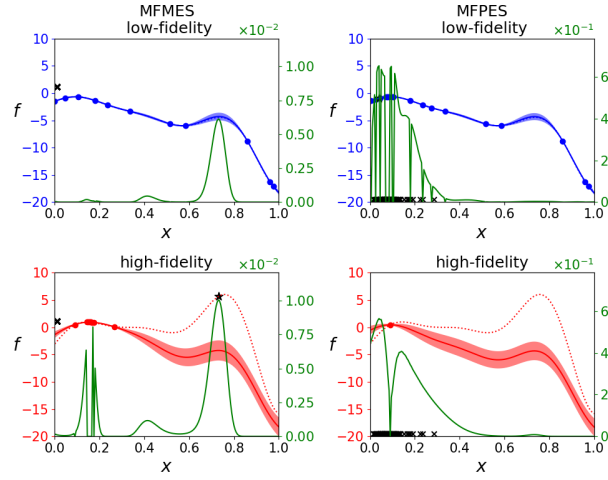
Figure 4 shows a typical example of behaviors of MF-MES and MF-PES on the Forrester dataset. Figure 4 (a) and (b) correspond to the iteration 5, and 10 at a trial, respectively. The left side shows MF-MES, and the right side shows MF-PES. The blue lines on the top row are the low fidelity function (dotted) and its GPR approximation (solid), and the red lines on the bottom row are the high fidelity function (dotted) and its GPR approximation (solid). The green lines are the acquisition function values, and the star represents a point which achieves the maximum of each acquisition function. Note that we set the acquisition function value for the already sampled point as 0. The number of samplings of f_* and x_* is set as 100, each of which is represented as the black crosses in each plot.

In the both methods, the local maximum around $x = 0.18$ strongly affects the sampled values of f_* and x_* . We see that the acquisition function of MF-PES is particularly sensitive to the location at which x_* is sampled. In the multi-fidelity setting, like this illustrative example, lower fidelity functions may have different argmax from the highest fidelity function, by which the estimation of $p(x_*)$ may be biased. In this iteration, MF-MES has higher acquisition function values for the true maximum compared with MF-PES despite that they have quite similar MF-GPR. In our experiments, empirically, MF-MES was relatively robust to this bias by considering the information gain of f_* instead of x_* .

As far as we observed, this problem in MF-PES was difficult to avoid even when the number of samplings is increased. Figure 5 shows the histogram of sampled x_* . Here, we generated 100000 samples by using the



(a) Iteration 5



(b) Iteration 10

Figure 4: Illustrative example on the Forrester function.

random feature map based MF-GPR obtained at iteration 10 of MF-PES. In this case, only one strong peak is still observed around 0.1, and the acquisition function of MF-PES can not have large values around the true argmax which is around $x = 0.8$.

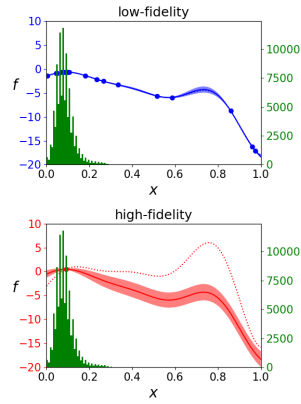


Figure 5: Histogram of sampled x_* . The same histogram is overwritten in the both of two plots for showing the relative location to the lower and the higher fidelity function.

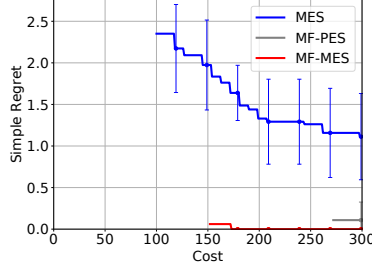


Figure 6: Simple regret on the three dimensional synthetic dataset. The average and standard deviation of 10 runs are shown.

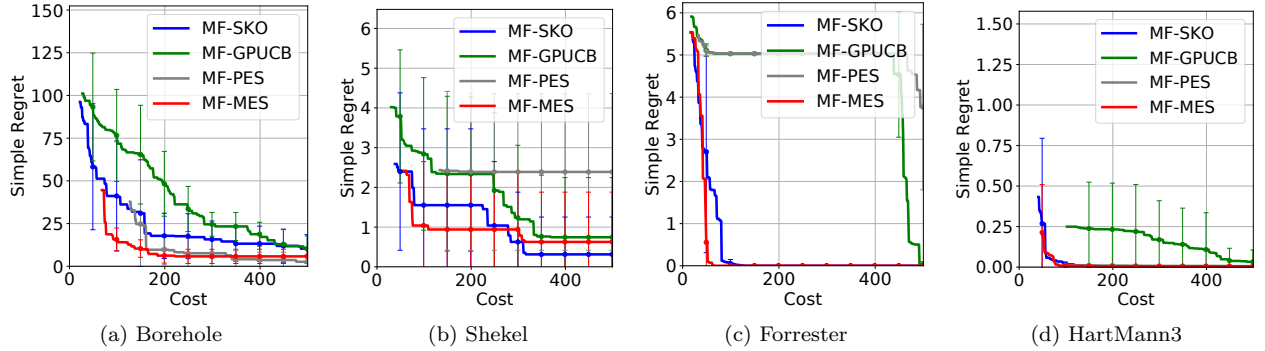


Figure 7: Simple regret on benchmark functions. The average and standard deviation of 10 runs are shown.

Appendix E Empirical Evaluation of Simple Regret

Simple regret is defined by $r_t = \max_{\mathbf{x} \in \mathcal{X}} f^{(M)}(\mathbf{x}) - \max_{\{i | i \in \{1, \dots, t\}, m_i = M\}} f^{(M)}(\mathbf{x}_i)$, which measures the best point queried so far. Figure 6, 7, and 8 show simple regret on synthetic, benchmark, and materials data, respectively. Note that to define simple regret, a highest fidelity observation is required for which MFBO methods may not have at the beginning of the optimization. Thus, the lines of the MFBO methods started from a cost at which each method queried at least one highest fidelity observation in all the 10 trials. All simple regret plots showed similar tendency to inference regret in the main text. In the materials dataset, MF-PES did not task any querying to the highest fidelity until the cost reaches the budget.

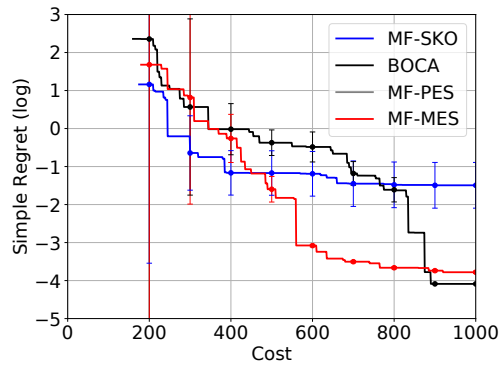


Figure 8: Simple regret on the materials dataset. The average and standard deviation of 10 runs are shown.